Melt compounding of polymeric nanocomposites

Utracki, L. A.; Sepehr, M.; Li, J.

Publisher's version / Version de l'éditeur:

International Polymer Processing, 21, 1, pp. 3-16, 2006-01-01

L. A. Utracki, M. Sepehr, J. Li*

National Research Council Canada, Industrial Materials Institute, Boucherville, QC, Canada

Melt Compounding of Polymeric Nanocomposites

The clay-containing polymeric nanocomposites (CPNC) can be visualized as binary mixtures of strongly interacting, inorganic, plate-like molecules dispersed in a polymeric matrix. To be successful, one must ascertain the thermodynamics, which controls CPNC structure on the molecular level. In this work dispersion of organoclay (Cloisite 15A, C15A) in polyamide 6 (PA 6) or in polypropylene (PP) is discussed. The PA-based CPNC's contained two components: polymer and organoclay, whereas those based on PP in addition contained a mixture of two maleated polypropylene's (PP-MA), as a compatibilizer. The melt compounding was carried out either in a single-screw extruder (SSE), or a twin-screw extruder (TSE). Both compounding lines were used with or without the extensional flow mixer (EFM). Furthermore, two versions of EFM were evaluated – one commercial, designed for polymer homogenization and blending, and the other designed for dispersing nano-particles. It was found that addition of EFM significantly improved clay dispersion. Better dispersion was found compounding the CPNC's in a SSE + EFM than in TSE with or without EFM. The best results were obtained using SSE with the new EFM having a relatively small gap between the convergent-divergent plates. C15A was fully exfoliated in PA 6 matrix. The results in PP/PP-MA matrix were less spectacular, but again the highest degree of dispersion was obtained using SSE + new EFM with a small gap. Tensile, flexural and impact properties were measured and evaluated.

1 Introduction

Polymeric nanocomposites (PNC) comprise polymeric matrix and dispersed in it particles, whose at least one dimension is smaller than about 10 nm. At present, the only nano-sized particles of interest to polymer industry are layered silicates, in particular natural (mineral) or synthetic clays, e. g., montmorillonite (MMT), or hectorite (HT). This article discusses the methods for dispersing individual clay layers or platelets in molten polymer, to form the clay-containing polymeric nanocomposite, CPNC.

Current industrial production of CPNC is based mainly on the reactive processes, i. e., polymerization of given monomer(s) in the presence of a pre-intercalated clay [1, 2]. Only the resin manufacturers able to dedicate a production line to CPNC may use this method. Development of reliable melt compounding technology will shift the CPNC manufacture from the resin producers to compounders and fabricators, i. e., where most multicomponent polymeric systems are being produced [3]. Melt compounding is applicable to any polymer/nano-filler system; it is rapid, environment friendly, and inexpensive. The technology will add flexibility; nanocomposites with desired performance characteristics will be prepared where and when needed. The advantages of the new technology will accelerate market acceptance of CPNC.

According to BCC, the global market for CPNC is over $ 200 million, increasing at a rate of 18.4 %/y. The consumption is projected to reach 550 k t/y by 2009 [4]. The main application is in the automotive industry (GM, Mitsubishi, Toyota), with a growing demand for packaging, appliances, building & construction, electrical & electronic, lawn & garden, power tools, sport equipment, etc. The cost between the neat polyamide and its CPNC is about 10 %.

Rheology distinguishes: (1) the shear flow with vorticity component, and (2) the extensional or irrotational flow. Most plastics compounders employ shear, while the theory shows that dispersing in extensional flow is advantageous [5]:

(1) It is orders of magnitude more energy-efficient (than shear).
(2) It generates better dispersive and distributive mixing.
(3) The temperature increases in extensional flow is low; ca. 1 to 3 °C.
(4) It does not cause re-aggregation of solid particles reported for shear.
(5) It can be economically generated using convergent-divergent flow geometry, either in motionless or dynamic mixing devices.

These were the reasons that lead to development of the EFM and its dynamic version, DEFM [6]. The device was designed for dispersing one molten polymer in another, i. e., for the preparation of polymer alloys and blends [7]. The EFM has been designed as an inexpensive mixer for blending molten polymers when attached to a single-screw extruder (SSE) [8]. This extruder is an efficient melting and pumping device, but poor mixer. Generating shearing flow, results in shear heating – local temperature increases by 70 °C have been measured. Alternatively, a twin-screw extruder (TSE) may be used. TSE is an excellent reactor and flexible compounder, but at manyfold higher capital and operational costs than SSE [9]. Since the pressure generated by TSE may be smaller than needed for EFM, a gear pump (GP) is usually used. Addition of GP to the compounding line not only increases the capital cost, but also induces additional processing and performance problems.

* Mail address: L. A. Utracki, National Research Council Canada, Industrial Materials Institute, 75 de Mortagne, Boucherville, QC, Canada, J4B 6Y4
E-mail: leszek.utracki@cnrc-nrc.gc.ca

For the preparation of polymer blends, the system SSE + EFM has been not only more economic, but often it outperformed TSE in such applications as elimination of gel particles in film resins, incorporation of elastomer into thermoplastics, or blending of two polymers such as PET with PP or PS with PE [4]. These results were expected on the basis of theoretical analysis of mixing, and indeed for melt homogenization, and melt blending EFM performs well. However, the principles of dispersing molten polymer drops are quite different from those of solid aggregates. Thus, it came as a surprise when several research teams reported that the commercial EFM-3 successfully dispersed organoclay in thermoplastic matrices (PET, PA 6, PP, and PS) [10 to 12]. The theory of mixing suggests that dispersion of solid particles should be four times more efficient in the extensional flow than in a shear field [13]. The preliminary results showed up to 70 % better performance. The postulated mechanism of organoclays dispersion required redesigning EFM. The results of comparative compounding will be discussed in this paper.

2 Fundamentals

2.1 Molecular Adsorption

Ideally, CPNC is a suspension of individual clay platelet in a polymer. The role of melt compounding is to ascertain such dispersion by delaminating organoclay stacks (exfoliation). The organoclay usually contains about 40 wt.% of intercalant, whose role is to facilitate the process. However, since the surface energy of crystalline solids is high, the intercalant adsorbed onto clay surface has low mobility, while the long-range polar interactions might cause formation of aggregates, with hundreds of aligned clay platelets. When matrix macromolecules directly graft to clay platelets, it is the polymer that is adsorbed. This has been the case for CPNC reactively exfoliated during polycondensation of ε-caprolactam. In such system containing 0.64 vol.% of clay there is 15 % less free volume (equivalent to the bulk reduction of temperature by > 50 °C) than in the matrix PA 6 [14]. Since the thickness of the adsorbed layer is about the same for polymers as that for low molecular weight organics [15 to 17], the reduced chain mobility is expected to be a general phenomenon, hindering the dispersion process. Owing to low thermal stability of organoclays, melt compounding of CPNC is usually carried out at the lowest possible temperature, generally insufficient for preventing formation of the solidified layer. The only solution of this conundrum is by the use of strong thermodynamic interactions, which would sufficiently increase the transition temperature.

Mathematical modeling of CPNC has been used to describe structure of polyamide (PA) based CPNC [18, 19]. The intercalant's ion charge was found dislocated and spread all over the molecule, causing it to stretch flat on the clay surface. The intercalant's hydrocarbon chains formed low-mobility, immiscible, isolating layer between clay and PA. Only local absence of intercalant could lead to thermodynamically favorable condition for clay dispersion. *Kim* et al. [20] considered CPNC composed of: clay, low molecular weight intercalant, macromolecular compatibilizer, and the matrix polymer. The computations showed the key role of thermodynamics for dispersing clay platelets in molten polymer – only when the thermodynamic conditions are satisfied the mechanical exfoliation may be achieved, i. e., the negative free energy of mixing is required:

$$\Delta G_m = \Delta H - T\,\Delta S < 0. \quad (1)$$

Since polymer diffusion into the gallery decreases the entropy, $\Delta S < 0$, the only way to satisfy the Inequality (Eq. 1) is for the enthalpy to be negative, $\Delta H < 0$. Thus, specific interactions are needed.

2.2 Melt Intercalation

Melt intercalation takes place during melt compounding in an extruder, internal mixer, or a similar device. Usually, the matrix polymer is melted first, and then compounded with a compatibilizer and intercalated clay under blanket of inert gas, e. g., N_2. Alternatively, the polymer is first mixed with a compatibilizer (e. g., its functionalized homologue) then compounded with intercalated clay. Industrially, CPNC is considered exfoliated when ≥ 80 wt.% of clay layers are uniformly dispersed in the polymeric matrix [2].

The dispersion mechanism in CPNC involves mechanical breakup of organoclay aggregates, followed by diffusion of macromolecules into interlamellar galleries. The latter process takes place even when the polymer radius of gyration is larger than the interlamellar gallery height:

$$d_{001} - 0.96 < \langle r_g^2 \rangle^{1/2} \cong 5 \text{ to } 40\,\text{nm}. \quad (2)$$

Evidently, the process must be motivated by a decrease of ΔG_m. Several mechanisms for the destruction of organoclay aggregates have been proposed, e. g., the "classical" aggregate rupture and erosion [21] or "peeling" [22]. While the equilibrium thermodynamics determines the potential for organoclays dispersion, the kinetics decides how far the process will progress. Two relations can be used as guides: (1) the self-diffusion coefficient, $D_s \propto 1/M_n^2$, and (2) the distance traveled by the diffusing macromolecules is proportional to the square root of the diffusion time, viz. $l_{diff} \propto t^{1/2}$. Evidently, mixing/compounding conditions affect the kinetics, but not the equilibrium thermodynamics (the effect of flow on miscibility is quite small [3]).

Melt intercalation/exfoliation belongs to the category of compounding multiphase polymeric systems, such as blends, composites, and foams [21, 23 to 25]. In dispersive mixers that employ shear, the vorticity components cause the flow elements (e. g., organoclay aggregates) to be repetitively stretched and compressed – the theory and experiments have shown that shear dispersion is only feasible when the ratio of the dispersed phase viscosity to that of matrix is low, $\lambda < 4$. Progress in the fundamental understanding of micro-rheology and laminar flow led to designing EFM for the production of polymer blends. These devices rely on the convergent-divergent flow, which repetitively stretches the flow elements in the flow and then in the transverse direction. The original EFM-1 [6] was a side-fed experimental unit, designed for rapid quenching of the melt inside for evaluation of morphology. However, at high feed pressures the mandrel tilted, causing asymmetric flow in

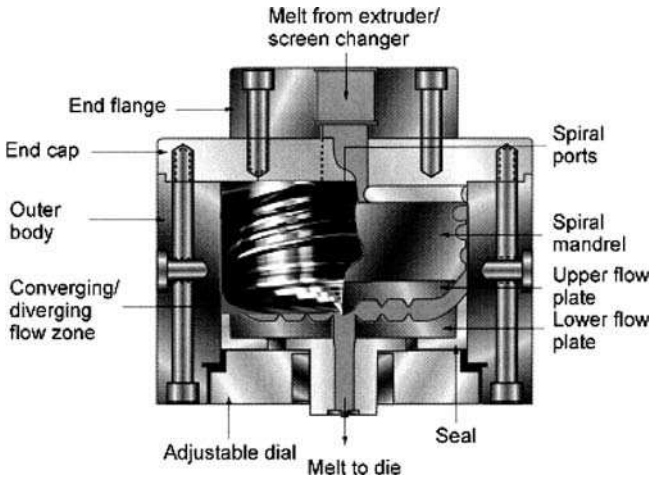

Fig. 1. The heart of the of EFM-3 is the converging/diverging (C-D) flow zone with the gap between the upper and lower plates adjusted by turning the adjustable die plate

the gap between the convergent-divergent plates. The EFM-2 used the spider axial feed. The symmetric flow design improved the ease of operation and performance, but at high feed pressures the "spider legs" had too high compliance. The commercial EFM-3 with the spiral mandrel feed geometry (see Fig. 1 [7]) is sturdy; the melt stream is efficiently homogenized, and uniformly distributed to the annular space around the convergent-divergent plates, with low-pressure loss. This design proved itself in the production lines with the mandrel diameter of up to 600 mm and throughput of ≤ 2 t/h [26].

In the patented dynamic version (DEFM) the SSE barrel and screw are extended. Depending on the need, the number of dispersive and distributive elements can be adjusted. Owing to the dynamic nature of the device the chances of unsymmetrical flow, and stagnant regions are eliminated. A simplified version of DEFM was designed, built, and tested for the dispersion of organoclay in polystyrene (PS) matrix. The results confirmed its superior clay-dispersing capability [27].

There is a need to redesign the EFM, adapting it for dispersing nanoparticles. Since the (shown in Fig. 1) EFM-3 passed industrial tests, the basic construction of the new unit (EFM-N) is the same; only the flow profile in the convergent-divergent (C-D) part have been modified. The new design is based on studies of flow and orientation of the nanoparticles, and deduced mechanism of clay aggregate dispersion. As before, the device forces the material to pass a series of C-D elements. Each element has three zones: a hyperbolic convergence that orient organoclay aggregates in the flow direction, a controllable gap were the lamellae are peeled off, and a divergent part that randomize the flow. The most critical is the balance of the extensional to shear stresses, engendered within this C-D part.

3 Experimental

3.1 Materials

A series of PA 6, or PP-based CPNC compositions was prepared with 0, 2, and 4 wt.% of Cloisite 15A (C15A, from SCP, Gonzales TX). For PP-based compounds in addition two PP-MA's were used, with different molecular weight and maleic anhydride (MAH) content; see Table 1.

3.2 Compounding Equipment

The compounding was carried out using a TSE, TSE + GP, TSE + GP + EFM, or a SSE with or without EFM. For comparison, EFM-3, and EFM-N, were used with at least four different gap settings between the C-D plates. To ascertain homogeneity, first a master-batch (MB) was prepared in a TSE, and then diluted in the aforementioned compounding lines. Owing to large volume of data and limited article length only a representative part will be presented and discussed here.

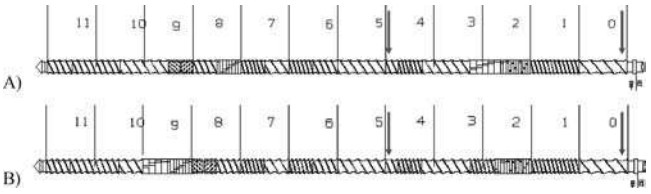

Fig. 2. Screw configuration for (A) PP/organoclay and (B) PA/organoclay. The polymer (and compatibilizer) was feed in zone 0, and organoclay in zone 5

Material	Trade name[1]	M_w kg/mol	Density g/ml	T_m °C	MAH wt.%	Supplier
PA 6	Ube-PA1015B	21.7	1.14	216	–	Ube Industries
PP	PROFAX-PDC1274	250	0.902	161	–	Basell Polyolefins
PP-MA1	Epolene-3015	47	0.91	162	1.31	Eastman Chemicals
PP-MA2	Polybond 3150	330	0.91	164	0.5	Crompton
Organo-clay[2] (C15A)	Cloisite® 15A	–	–	–	–	South. Clay Prod.

[1] Abbreviations used in the text (from top): PA 6, PP, E3015, P3150, and C15A
[2] C15A is MMT intercalated with excess (1.25 meq/g or 0.78 mmol/g) of di-methyl di-hydrogenated tallow ammonium chloride (Arquad 2HT); it contains 43 wt.% of the organic phase and 2 wt.% of water

Table 1. Material characteristics

System	Temperature, T (°C)		Pressure, P (MPa)		Cooling time (s)
	Barrel	Mold	Injection	Holding	
PA/C15A PP/C15A	250 200	55 40	65 52	6 5	21 30

Table 2. Molding conditions for CPNC with PA or PP as the matrix

The TSE was Leistritz-34 mm CORI, L/D = 40, and screw configuration shown in Fig. 2. Compounding was done under dry N_2 at the screw speed of $N = 200\ min^{-1}$, throughput of Q = 5 and 10 kg/h, at the temperatures of T = 180 and 200 °C for PP, or 240 °C for PA systems. Gear Pump (GP) was from Maag Pump System Model EH 45/28; capacity 5 to 100 kg/h; T up to 290 °C; suction pressure to 20 MPa, discharge pressure to 70 MPa. SSE was Flag 63.5 mm machine with L/D = 24, and a two-stage screw with dry element. EFM-3, or EFM-N was used with the C-D gap settings: h = 5 to 2000 µm. Test ASTM specimens (D638, Type I, D790 and D256) were injection-molded in Engel 150T machine using ASTM end-gated mold. The conditions are listed in Table 2.

3.3 Residence Time Distribution (RTD)

The in-line measurements of the residence time (t_R) and its distribution (RTD) during extrusion compounding at the throughput of $Q \cong 5$ kg/h were conducted at ultrasonic (US) frequency of 5 MHz [28]. For the tests, a small amount of $CaCO_3$ was used as a tracer. The mean residence time is listed in Table 3. It is noteworthy that while in TSE the throughput is controlled by the feed rate, in SSE this is accomplished by changes of the screw speed (see Fig. 3). Thus, while t_R in TSE changes with flow restrictions in the die region, in SSE it is about constant; $Q = 5.21 \pm 0.33$ kg/h. Evidently, doubling Q to 10 kg/h, reduced t_R by half. In both compounding lines, flow restriction in the die region broadens the residence time distribution.

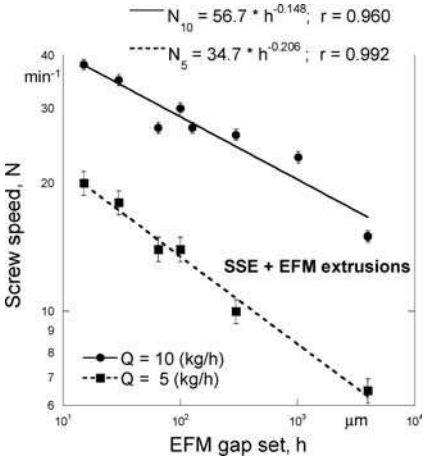

Fig. 3. Correlation between EFM-3 gap setting, h, and SSE screw speed, N

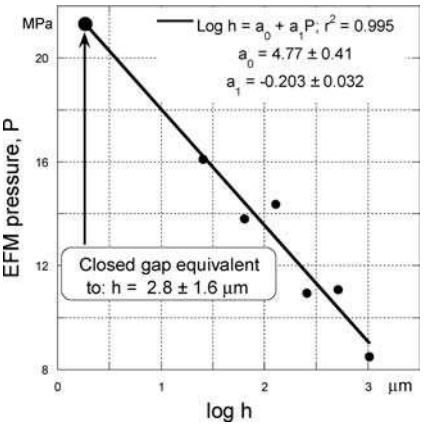

Fig. 4. Pressure vs. EFM-3, gap h = 0 to 1 mm – semi-logarithmic fit to determine equivalent gap for closed EFM

Twin-screw extruder (TSE)		Single-screw extruder (SSE)	
System	t_R (s)	System	t_R (s)
TSE TSE + GP TSE + GP + EFM open TSE + GP + EFM closed	139 236 320 368	SSE – SSE + EFM open SSE + EFM closed	1163 – 1147 1108

Table 3. Time to attenuation peak during compounding at constant throughput of Q = 5 kg/h in TSE or SSE compounding lines

The pressure in EFM-3 as a function of gap, h (μm), between the C-D plates is shown in Fig. 4. Extrapolation to the pressure read when the gap was fully closed gives $h = 2.8 \pm 1.6$ μm. Since the precision of machining is rarely better than ±5 μm, the extrapolated value indicates good machining and alignment of the C-D plates.

3.4 Compounding

The master batch (MB) ingredients (70 wt.% PP with 10 wt.% of E3015, P3150, and C15A each) were dried at 90 °C for 12 h in a commercial drying tower. The compounding was carried out at Q = 5 or 10 kg/h, feeding PP + compatibilizers from the main hopper, and C15A from a side-feeder. Next, the MB was diluted to 2 or 4 wt.%, using either TSE or SSE with or without EFM.

Similarly, PA 6 and C15A were dried respectively for 48 h at 80 °C and overnight at 100 °C. The MB (96 wt.% PA 6 with 4 wt.% C15A) was prepared in a TSE at Q = 5 kg/h. Next, the MB was either re-passed through a compounding line, or diluted to 2 wt.%.

3.5 Characterization

The injection molded ASTM-type specimens for mechanical testing contained 0, 2, and 4 wt.% organoclay. The specimens for XRD, SEM, and TEM were prepared by cutting dogbone in the middle, and selecting the central part for the test.

3.5.1 Evaluation of Clay Dispersion

The XRD measurements were carried out using a Brüker D8 Discover with CuKα radiation (wavelength $\lambda = 0.15406$ nm, at a scan rate of 0.3°/min, with slits of 1, 0.1, and 0.6 mm. From the spectra three measures of the degree of dispersion were calculated: (1) the main interlayer spacing, d_{001} (see Eq. 3), (2) the number of platelets per stack (see Eq. 4), and (3) the amount of clay platelets absent in stacks. The latter calculations were based on the numerical integration of the area under the peak, compared to that under the peak of a given organoclay [29].

The main diffraction peak position may be calculated from Bragg's formula:

$$d_{00n} = n\lambda/(2\sin\theta), \tag{3}$$

where, n is an integer, θ is the angle of incidence (or reflection) of X-ray beam. From the peak broadening the thickness of the diffracting clay stack, t_S, was calculated using Scherrer relation. Knowing this value and d_{001}, the number of clay platelets per average stack are:

$$m = 1 + t_S/d_{001}, \text{ where: } \quad t_S \cong 0.9\lambda/(B_{1/2}\cos\theta_B). \tag{4}$$

In Eq. 4 $B_{1/2} \cong (\theta_1 - \theta_2)$ is the peak width at half height ($I_{max}/2$), and $\theta_B \cong (\theta_1 + \theta_2)/2$.

The samples were observed under height resolution TEM (Hitachi H9000), and SEM (Hitachi S4700 with cold field emission gun, FEGSEM). The specimens were prepared by shaving ca. 70 nm thick sections from the dogbones at room temperature using a Leica Ultracut FC microtome with diamond knife.

For SEM some specimens were fractured, while others were polished, and chemically treated. The aim was to check for the presence of large aggregates, even when the HRTEM showed well-dispersed platelets.

3.5.2 Mechanical Properties

Before the tests, the PA 6 specimens were dried under vacuum at 50 °C for at least 31 days, those of PP overnight at 90 °C. The tensile and flexural tests (ASTM D638 and D790, respectively) were carried out using an Instron 5500R model 1125 tester at the crosshead speed of 5 and 15.7 mm/min, respectively. An extensometer was used to measure the strain. Young's modulus was calculated by least squares fitting of the experimental stress vs. strain data, within the initial strain region of < 0.2 %. For the flexural tests the support span was 59 mm. Notched Izod impact tests (ASTM D256) were performed at room temperature using an impact tester Instron Model 8200. The values reported here are averages of at least ten tests for each specimen.

4 Results

4.1 Clay Dispersion in PA 6 Matrix

Examples of the X-ray scan for CPNC compounded in TSE or SSE are shown in Figs. 5 and 6, respectively. The compounding conditions and the XRD results are listed in Table 4. The SSE with EFM-N produced the highest degree of clay dispersion in PA 6 matrix. The apparent lack of diffraction peaks in Fig. 6 indicates absence of ordered alignment of clay platelets. Good dispersion is also evident in the HRTEM micrographs in Fig. 7.

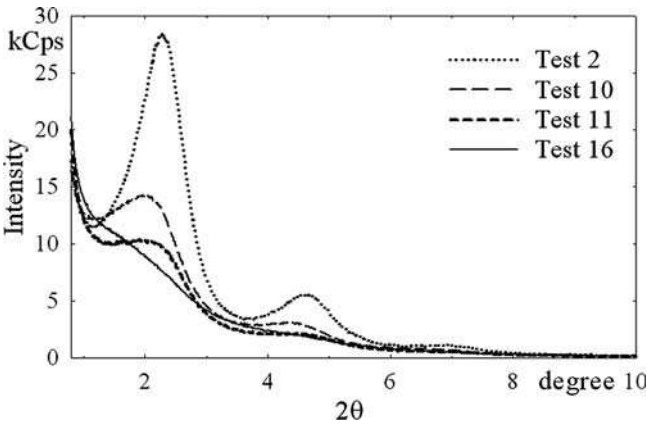

Fig. 5. XRD of PA 6 with 2 wt.% C15A compounded in TSE (medium shear screw configuration), TSE + GP, or in TSE + GP + EFM-3 (gap of 5 μm). For the compounding conditions see Table 4

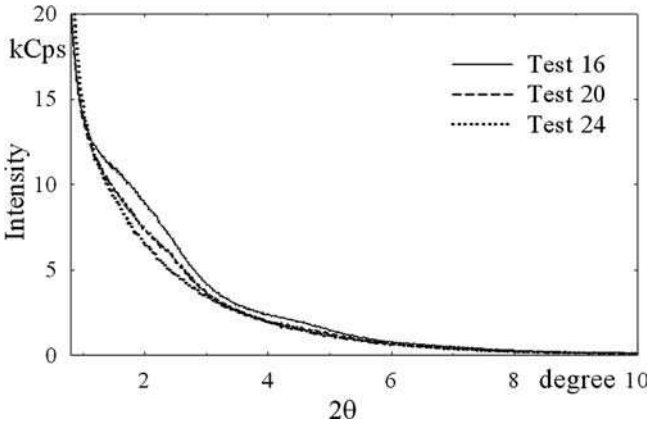

Fig. 6. XRD of PA 6 with 2 wt.% C15A compounded in SSE with either EFM-N (bottom curve) or EFM-3, both with gap of 30 μm. For comparison the best result from Fig. 5 (test # 16) is also shown

4.2 Mechanical Properties of PA 6-based PNC

To avoid changing the crystallinity of the sample, the injection molded CPNC specimens were dried under vacuum at 50 °C for 32 days. The results of the tensile, flexural and impact tests are listed in Table 5. For comparison, the corresponding values determined for the commercial CPNC, Ube PA1015C2 (containing 2 wt.% organoclay) are also presented in Tables 4 and 5.

4.3 Clay Dispersion in PP Matrix

The XRD measures of clay dispersion are summarized in Table 6, and the test results are shown in Figs. 8 and 9. The compounding was carried out at T = 180 °C. The dispersion does not correlate with the compounding conditions. This is particularly evident for the interlayer spacing, d_{001}, and the number of clay platelets in the residual stacks, N. However, Δex systematically increases with reduction of EFM gap. It is noteworthy that for these systems Δex (%) was calculated as the additional exfoliation engendered by EFM, i. e., above that in samples compounded in TSE or SSE alone.

The XRD results were confirmed by FEGSEM and HRTEM. The former showed that in CPNC prepared using EFM-N (with gap h $\leq$ 63.5 μm) C15A stacks were uniformly dispersed (absence of aggregates). The HRTEM micrographs (see Fig. 10) indicated that compounding in SSE + EFM-N resulted in better dispersion than that in TSE + GP + EFM-3. In summary, for PP-based CPNC's EFM caused: (1) reduction of clay aggregates, (2) enhanced exfoliation, and (3) reduction of d_{001}.

4.4 Mechanical Properties of the PP-based PNC

Results of the tensile, flexural and impact tests are presented in Table 7. Since the mechanical behavior of semi-crystalline polymers depends on crystallinity, a DSC was used to measure the total crystallinity in the injection-molded, undeformed spe-

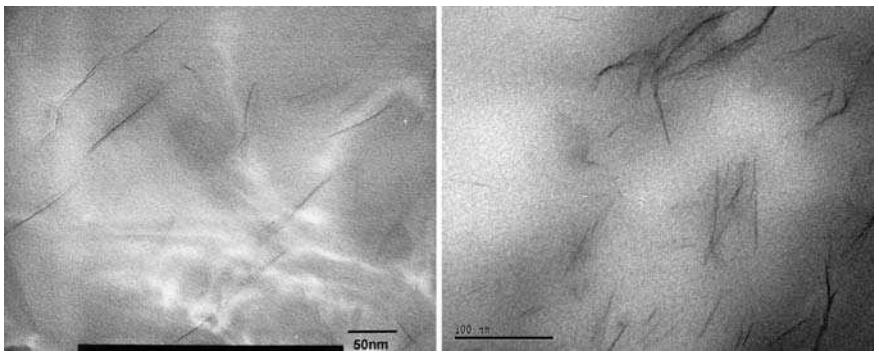

Fig. 7. HRTEM micrographs (200 k) of PA 6 with 2 wt.% C15A: left micrograph is for test #16 (TSE + GP + EFM 5 μm gap), right micrograph is for #24 (SSE + EFM-N 30 μm gap)

Test #	C15A wt.%	Specimen (compounder)	EFM gap,h μm	Interlayer spacing, d_{00n} (nm)		Platelets/stack N	Total exfoliation ex (%)
				Main peak	Secondary peak		
1	100	Cloisite® 15A	–	3.21	1.95/1.22	3.34	–
2	4	Master-batch	–	3.87	1.91	3.35	–
10	2	TSE	–	4.44	1.98	2.79	52.7
11	2	TSE + GP	–	4.42	2.02	2.89	64.7
16	2	TSE + GP + EFM-3	5	4.39	1.94	2.78	83.3
20	2	SSE + EFM-3	30	3.65	1.81	3.14	89.9
24	2	SSE + EFM-N	30	4.65	1.91	2.15	97.1
26	2	UBE1015C2	–	5.33	–	2.15	80.7

Table 4. Summary of the XRD scans for PNC's based on PA 6. To ascertain reliability of data up to four measurements were taken for each composition – the reported values are averages. The average error of measurements for d_{00n} is ± 0.01, for the number of pellets per stack is ± 0.22, and for the degree of exfoliation is ± 3.5 %

Test #	Tensile tests (ASTM D638)			Flexural tests (ASTM D790)		Impact strength J/m (ASTM D256)
	Modulus GPa	Strength MPa	Elongation %	Modulus GPa	Strength MPa	
2	3.58	78	59	3.40	135	28
10	3.37	80	82	3.47	152	24
11	3.37	82	163	3.46	152	21
16	3.32	82	145	3.61	155	25
20	3.73	91	123	3.61	151	29
24	3.77	90	93	3.62	151	26
26	3.80	94	94	3.92	165	24

Table 5. Mechanical properties of PA 6 based PNC. Compounding conditions are listed in Table 4. The average error of measurements for the tensile modulus, strength and elongation was ± 2, 4, and 5 %, respectively; that for the flexural modulus, and strength was ± 4, and ± 5 %, respectively, while the average error of measurements for the impact test was ± 12 %

Test #	C15A wt.%	Specimen (compounder)	EFM gap, h μm	Interlayer spacing, d_{00n} (nm)		Platelets/stack N	Excess exfoliation Δex (%)
				Main peak	Secondary peak		
1	100	Cloisite® 15A	–	3.21	1.95/1.22	3.34	–
27	10	Master-batch	–	3.52	1.30	2.59	–
33	4	TSE + GP + EFM-3	63.5	3.17	1.35	2.83	18.1
35	2	TSE	–	3.57	1.35	2.59	0
36	2	TSE + GP	–	3.47	1.34	2.74	2.0
40	2	TSE + GP + EFM-3	15.0	2.95	1.34	2.79	28.9
45	2	SSE + EFM-3	15	3.32	1.35	3.10	27.1
49	2	SSE + EFM-N	15	3.09	1.35	3.00	28.7

Table 6. Summary of the XRD measurements for PP-based PNC containing X wt.% C15A and 2X wt.% of compatibilizers. To ascertain reliability of data up to four measurements were taken for each composition – the reported values are averages. The average error of measurements for d_{001} is ± 0.003 nm, for the number of pellets per stack is ± 0.04, and for the degree of exfoliation is ± 1.2 %

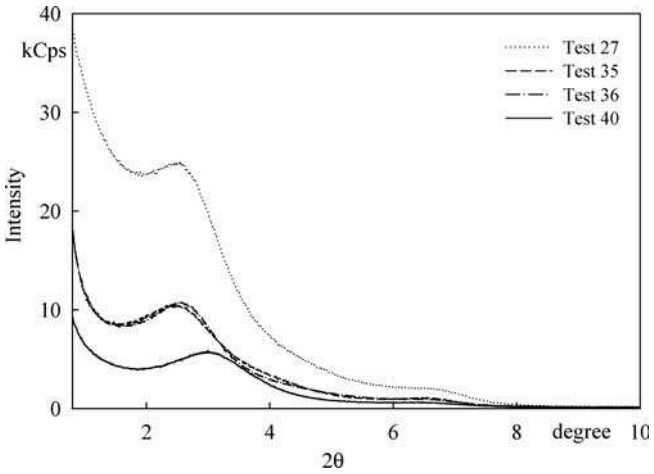

Fig. 8. XRD of PP with 2 wt.% C15A and 4 wt.% PP-MA compounded in TSE, TSE + GP, and TSE + GP + EFM-3 (gap of 15 μm). XRD of MB is also shown

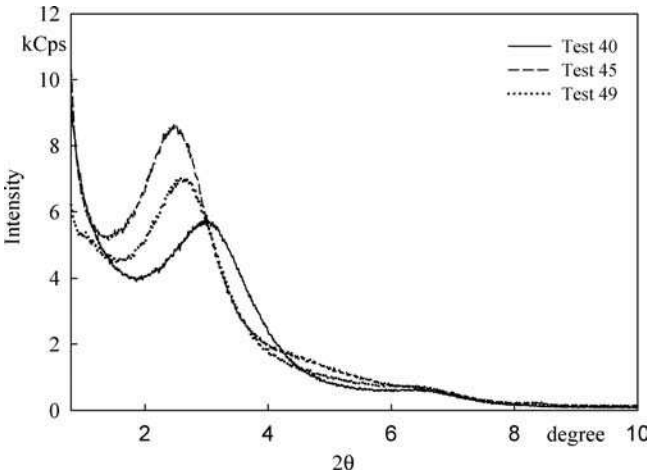

Fig. 9. XRD of PP with 2 wt.% C15A and 4 wt.% PP-MA compounded in SSE with either EFM-N or EFM-3 (gap = 15 μm) compared to TSE + GP + EFM (test #40)

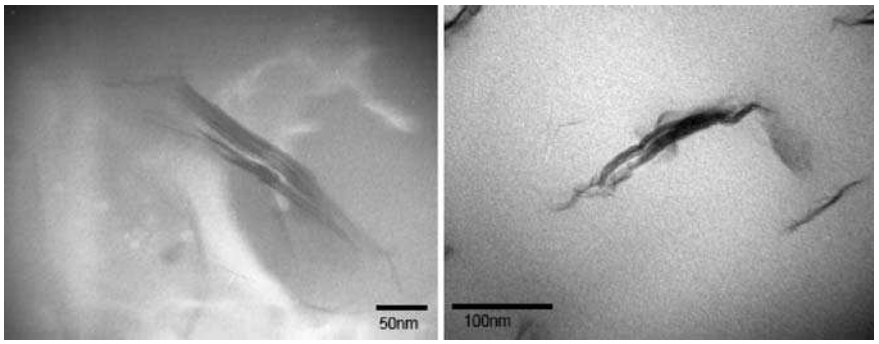

Fig. 10. HRTEM micrographs (200K) of PP with 4 wt.% PP-MA compatibilizers and 2 wt.% C15A. (Left) compounded in TSE + GP + EFM (15 μm), and (right) in SSE with EFM-N (gap of 15 μm)

Test #	Tensile tests (ASTM D638)		Flexural tests (ASTM D790)		Impact strength J/m (ASTM D256)
	Modulus GPa	Strength MPa	Modulus GPa	Strength MPa	
27	2.94	32	2.34	56	15
33	2.16	33	1.82	57	31
35	2.09	33	1.90	60	19
36	2.15	33	1.84	59	23
40	2.07	34	1.92	61	33
45	2.09	35	2.07	59	35
49	2.08	36	2.11	59	34

Table 7. Mechanical properties of PP based PNC. Compounding conditions are listed in Table 6. The average error of measurements for the tensile modulus, and strength was ± 4, and ± 5 %, respectively; that for the flexural modulus, and strength was ± 4, and ± 5 %, respectively, while the average error of measurements for the impact test was ± 12 %

cimens, the same that were used in the tensile and impact strength tests. It was found that independently of the processing conditions the total crystallinity was 43 ± 2 wt.% and the melting point was: T_m = 164.5 to 165.5 °C. Thus, the presence of organoclay and compatibilizers had little effect on PP crystallinity.

5 Discussion

5.1 Melt Intercalation in PA Matrix

Most processes labeled as "melt intercalation" start with pre-intercalated clays. In 1996, *Maxfield* et al. [30] compounded in TSE a PA 6 with MMT-2M2ODA, and a silane sizing agent [31, 32]. Similarly, *Liu* et al. [33] melt intercalated PA 6 with MMT-ODA. These preparations did not result in exfoliation.

Dennis et al. [22] published results of m the most thorough investigation of melt compounding of PA 6 with either Cloisite 30B (C30B; MMT-MT2EtOH) or C15A. PA 6/C30B readily exfoliated in an intermeshed counter-rotating TSE (ICRR), but since the goal was to examine the relative merits of compounding methods, the authors focused on the more discriminating PA 6/C15A system.

Several extruders were used, viz. SSE and TSE (CORI, ICRR, and CRNI-type) with several screw configurations. The XRD peak position did not change much (d_{001} = 3.2 to 3.8 nm), but the degree of dispersion (DD; determined from TEM) correlated with average residence time, $\bar{t}$, and the variance of the residence time distribution, σ_a^2:

$$DD = -4.2 - 0.21\bar{t} + 564\sigma_a^2 + 0.0017\bar{t}^2 - 4100(\sigma_a^2)^2; \quad r = 0.98, \tag{5}$$

where r is the correlation coefficient. The best dispersion was obtained using a medium shear screws, with long residence time. Furthermore, DD correlated with the tensile modulus and yield strength, but not with the impact strength or elongation at break [2]. Similar results were obtained by other authors [34 to 41] – compounding in TSE a PA 6 with C30B-type organoclay resulted in exfoliation, whereas those with C15A-type in intercalation. The mechanical performance was poor, sometimes decreasing with clay content [37]. The extrusion was also reported to reduce the interlayer spacing from d_{001} = 1.81 nm of the organoclay, down to about d_{001} = 1.3 nm in the product [41].

Thus, exfoliated PNC are being manufactured either employing reactive processes [42, 43] or compounding PA with organoclays having ethoxy groups. By contrast, compounding PA with organoclays pre-intercalated with paraffinic-type intercalants invariably leads to intercalated systems, and small (if any) enhancement of performance.

5.2 Melt Intercalation in PP Matrix

Initial attempts to produce PP-based CPNC followed the technology developed for PA, namely by polymerization of olefinic monomers in the presence of intercalated clay platelets.

Alternatively, it was proposed to incorporate ammonium ions at chain ends either of the main or a side chain of a PO macromolecule [2]. However, both approaches were found impractical.

The 1999 patent from Toyota [44], and several articles [45 to 48] describe the current technology. Originally, these nanocomposite were prepared compounding PP with MMT-ODA and a "guest molecule" with a polar group, e. g., hydroxyl or anhydride. It has been postulated that exfoliation in the system involves grafting PP-MA macromolecules by means of some reaction involving maleic anhydride (MAH) groups. Recently, in the PP/PP-MA/C15A system a reaction between MAH and hydroxyls on the clay surface has been detected by FTIR [49]. It is noteworthy that MAH groups have the tendency of forming clusters in the PP matrix. Thus, if grafting is to take place the intercalant has to be partially removed from the clay surface, the MAH clusters broken, and the MAH groups must be able to react with clay surface before the platelets re-aggregate. When the rate of organoclay degradation is greater than that for cluster breakup and the MAH reaction, re-aggregation of clay platelets is observed, while for the reversed case a progressive exfoliation is expected. Fig. 11 indicates that these processes may take place simultaneously. Possibly, the outer platelets that are easier to peel off may in time react with MAH groups

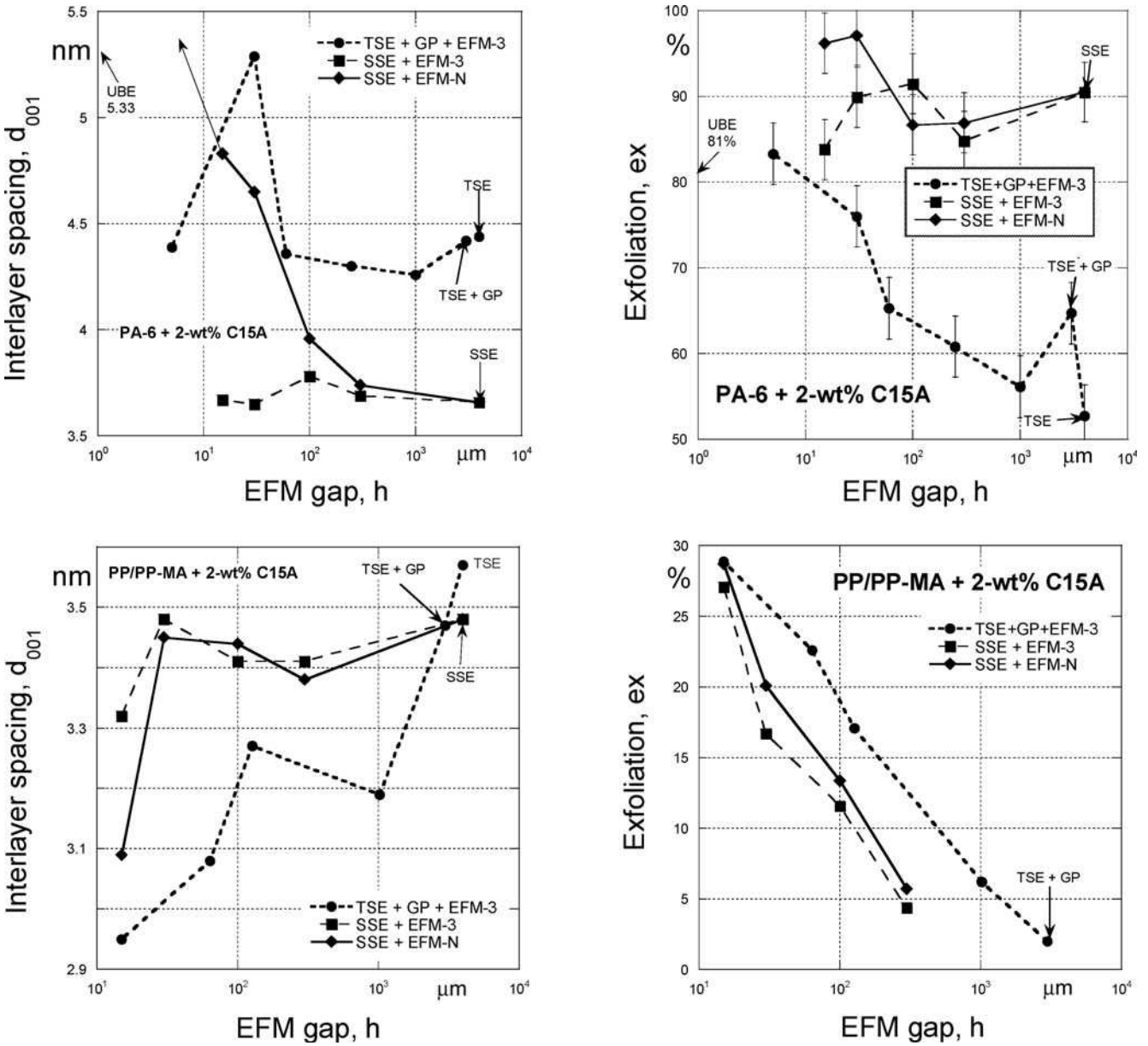

Fig. 11. Clay dispersion in CPNC as measured by the interlayer spacing (left column) and the degree of exfoliation (right column). Results of compounding in a TSE + GP + EFM, and in SSE with either EFM-3 or EFM-N are shown for PA 6 (top row) and PP (bottom row) systems. Arbitrarily the gap for the extruder alone was set as 4 mm, and that for TSE + GP as 3 mm. The other data points are as determined. For comparison, the values for the standard Ube PA1015C2 are also shown in the top row. The error bar for d_{001} (0.01 nm) is invisible, that for exfoliation (3.5 %) is the same for PA 6 (shown) and for PP system

and exfoliate, whereas within the stacks the C15A layers degrade faster than PP-MA diffuses into the interlamellar galleries and interact with clay.

During the last decade, the original strategy for the preparation of PP-based CPNC has been critically evaluated using a variety of organoclays, and compatibilizers [45 to 54]. For example, natural or synthetic clay was pre-intercalated with HAD, DDA, ODA, 2MHDODA, 2M2ODA, 2M2HTA, MT2EtOHA, 2MHTL8A, 3MHDA, and others. Oligo- or poly-propylene's modified with hydroxyl, acidic, acid anhydride, or epoxy groups have been used as compatibilizer. Good results were obtained with PP-MA of relatively high molecular weight, containing low MAH content (ca. 0.5 wt.%) [50], or with PP grafted with glycidyl methacrylate (PP grafted with acrylic acid was less efficient). Three critical factors for clay exfoliation have been identified: (1) miscibility of compatibilizer with PP matrix [45, 48]; (2) the weight ratio of the compatibilizer to organoclay [47]; and (3) the local clay concentration (after crystallization of the matrix). Owing to the cost and availability, the compatibilizer of choice is PP-MA. For example, the MMT interlayer spacing for the compatibilizer-to-organoclay ratio of 1 : 1 was $d_{001} \cong 3.28$ nm, while for 10 : 1 the XRD peak disappeared altogether, indicating exfoliation. Melt compounding of lightly maleated PO with pre-intercalated clay resulted in high degree of dispersion [51 to 52]. Thermal stability of the intercalant [53] plays an important role. The degradation depends on the chemical nature of the intercalant, e. g., MMT intercalated with 2M2HTA is more stable than that with MT2EtOH [2, 54]. Elimination of intercalant from the clay surface facilitates access of MAH-groups to the clay hydroxyls, but it may reduce the interlayer gallery heights, thus hindering infusion of the macromolecular species.

5.3 Clay Dispersion in PA 6 and PP Matrices

The data presented in Figs. 5 and 6 show that the use of EFM in either the TSE, or SSE compounding lines significantly improves the degree of clay dispersion in PA 6. As evident from data in Table 3, varying the gap between C-D plates has insignificant effect on the residence time, but substantial on the clay dispersion. Thus, in the discussed experiments not the residence time but the flow geometry and related to its intensity and type of the stress field control dispersion. The flow in EFM has three components: the planar elongational flow at the entrance to the convergent-divergent (C-D) gap, the shear flow inside it, and the orthogonal extensional flow at the exit. The organoclay stacks are oriented at the entrance to C-D gap, they are forced to peel by the sharp velocity gradient within the gap, and then they are "pulled apart" in the divergent part of C-D. The process is efficient and rapid, repeated several times before the melt exits from the device.

As the data in Tables 4 and 6 show, in PA and PP systems compounding leaves behind short stacks of about 2 to 3 clay platelets. In agreement with the reported observations [22], the main XRD interlayer spacing varies but little; for PA 6 system from 3.21 to 5.29 nm, with the mean value of $d_{001} = 4.09 \pm 0.44$; and for PP-based one from 2.95 to 3.57 nm, with the mean value of $d_{001} = 3.30 \pm 0.04$. The degree of dispersion is mainly reflected in the reduction of the primary peak intensity; hence in the reduction of the number of aligned, diffracting platelets. There are several causes for such a reduction, e. g., exfoliation, misalignment, and orientation being the main. However, on the basis of extensive HRTEM studies (see Figs. 7 and 10) it is evident that exfoliation is the main mechanism.

Along with the newly prepared CPNC's, the commercial nanocomposite (the widely used as a reference Ube PA1015C2) was also studied. The latter material has been prepared by dispersing MMT pre-intercalated with ω-amino dodecanoic acid in caprolactam, and then initiating the ring opening polycondensation. Thus, the intercalant molecule becomes the first unit of the PA 6 chain that ionically bonds it to the clay surface [55]. The system is exfoliated, and it has excellent properties [56]. Structurally, the compounded CPNC of PA 6 with C15A is quite different; the 2M2HT intercalant is thermodynamically immiscible with PA 6, thus it is a barrier for the interactions between clay and the polymer. To create favorable condition [18 to 20], two processes must take place: a partial removal of intercalant, and interaction of PA 6 macromolecules with the clay surface.

Dissolution of the excess 2M2HT of C15A into molten PA 6, followed by Hofmann elimination [53] may account for the former process. During the static intercalation, the second process would favor low molecular weight components. During compounding [37, 39, 40] not the molecular diffusion, but mechanical peeling of partially bare clay platelets from the stacks dominates the dispersion process [22] – EFM facilitates the peeling process. Once the partially bare clay platelets are peeled off the stacks, the thermodynamic interactions between them and polar chains (PA 6 or PP-MA) may take place; hence the rate of reactive species diffusion to the bare platelet must be faster than the re-aggregation of clay platelets, which is easier to achieve in polar PA 6 system than in the one with PP-MA dispersed in PP as the matrix.

Fig. 11 illustrates variation of the two main parameters that characterize clay dispersion for the two types of CPNC's and three compounding lines. The upper two complementary graphs display variation of the interlayer spacing, d_{001}, and exfoliation, ex, for the PA 6/C15A system. Different flow fields in these compounding lines are responsible for the different relations between d_{001} (or ex) and EFM gap. To include the data for compounds prepared without EFM, an arbitrarily ordinates were selected: for the extruder alone: h = 4, whereas for TSE + GP: h = 3 mm. The flow through TSE is energetic – it generates higher interlayer spacing than SSE, but less exfoliation. Reducing the EFM gap to below 60 μm initially increased d_{001} than (due to intercalant degradation) it decreased. Compounding in SSE + EFM-3 engenders different performance than that in SSE + EFM-N. For both lines the extent of exfoliation is high – at least as high as that measured for Ube PA1015C2. For gaps < 100 μm superiority of EFM-N is evident – to the eye the diffraction curves are featureless (see Fig. 6), but the numerical analysis gives the value of ex = 96 %. The superiority of EFM-N is also evident in the plot of d_{001} vs. h – while the reduction of EFM-3 gap hardly affects the gallery height, for EFM-N it causes a progressive expansion. The XRD peak becomes not measurable for gaps smaller than 30 μm.

The tendencies for PP-based CPNC's are different from those of PA-based ones. Here, the thermal instability of C15A

dominates. As before (see Fig. 11), TSE causes the greatest reduction of d_{001} as a function of decreasing h. In SSE + EFM degradation is evident only for the smallest gap of 15 μm. However, in all three compounding lines the gap reduction improves the dispersion – ex increases with reduction of h, the strongest for SSE + EFM-N.

5.4 Relation between the Clay Dispersion and CPNC Performance

Several measures of CPNC mechanical behavior are listed in Tables 5 and 7. Since the results obtained in tensile and flexural tests are proportional to each other, only the tensile and impact properties will be discussed. For the best CPNC's, the relative modulus, $E_R = E_{CPNC}/E_{matrix}$, increases with clay content, w, following an empirical dependence [2]:

$$E_R \simeq 1 + 0.2w. \quad (6)$$

Thus, for the series of CPNC's with 2 wt.% C15A (1.14 wt.% clay) the Young's modulus is expected to increase by about 23 %. Depending on the molding conditions, the modulus of the PA 6 used in this study ranges from $E_m = 2.7$ to 3.0 GPa [55 to 57]; hence that of its CPNC is expected to be $E_c \leq 3.5 \pm 0.2$ GPa. Similarly, since E_m of PP with 4 wt.% PP-MA was determined as 1.73 ± 0.1 GPa, the value for its CPNC modulus should be: $E_c \leq 2.1 \pm 0.1$ GPa. As the data in Tables 5 and 7 show, the maximum experimental value for PA 6 and PP-based CPNC with 2 wt.% C15A is 3.8 ± 0.2 and 2.2 ± 0.1 GPa; hence close to the expected values for both systems. Since the maximum effect is expected for the fully exfoliated system, Fig. 12 displays the relation between the relative Young's modulus, E_R, and the extend of exfoliation. A similar dependence was obtained for E_R vs. d_{001} plot (not shown). The data points fall into three groups: the lowest values of dispersion and E_R were obtained for PP-based CPNC, while these for PA 6 type CPNC form two distinct groups – all samples prepared in TSE compounding line show low relative modulus, $E_R < 1.25$, while all those prepared in SSE have $E_R > 1.25$. Within the latter group the samples prepared with SSE + EFM-N show the highest values.

Tables 5 and 7 list also data for CPNC with 4 wt.% C15A, prepared using the TSE compounding line. According to Eq. 6, the expected enhancement of modulus for the fully exfoliated system should be 46 %, i. e., $E_c(PA) = 4.2 \pm 0.2$ GPa, and $E_c(PP) = 2.5 \pm 0.1$ GPa. Evidently, these values are higher that those observed (ER = 3.6 and 2.2 GPa, respectively), as due to crowding, the clay platelets cannot be exfoliated – low values for ex are reported for both CPNC systems.

Fig. 13 displays the relative tensile strength, σ_R (error bars of ±4 %), of CPNC with 2 wt.% C15A in PA 6 or PP + PP-MA as the matrix vs. the degree of exfoliation. Placing the values for PA 6 and PP CPNC's on the same Figure does not imply common dependence. Plot of tensile strength vs. clay content often shows the opposite tendency than the modulus [2]. Most frequently the reversal was observed for organoclay loading exceeding some critical value (usually 4 to 6 wt.%), where the degree of dispersion becomes too low.

The tensile strength, σ, is more difficult to predict than the modulus. Strength involves transmission of stresses through the tested specimen, thus it must depend on the degree of exfoliation, type of bonding between clay platelets and the matrix, as well as on the matrix. The simplest case is for the continuous particles that perfectly adhere to the matrix. The tensile strength in the stress direction is expected to follow the volumetric rule of mixtures [58]:

$$\sigma_R \equiv \sigma_c/\sigma_m = 1 + \varphi_f(\sigma_r - 1); \quad \sigma_r \equiv \sigma_f/\sigma_m, \quad (7)$$

where φ is the volume fraction, and the subscripts c, m and f stand for composite, matrix, and filler, respectively [2]. Eq. 7

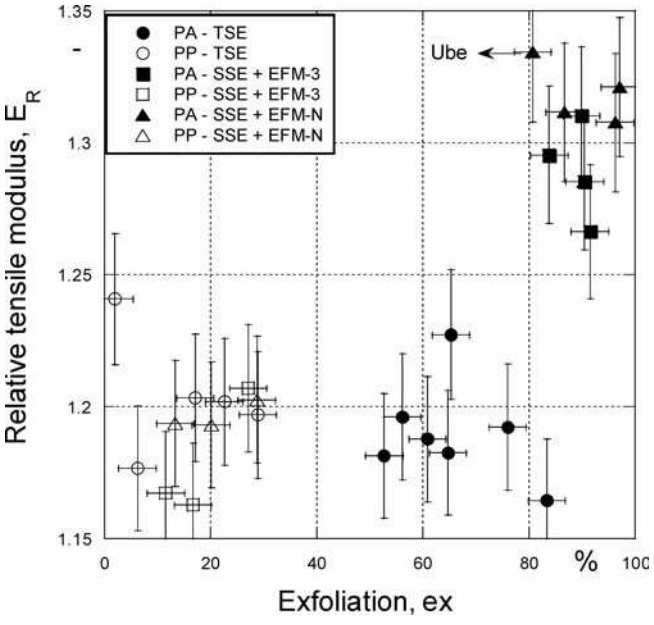

Fig. 12. Relative modulus of CPNC containing 2 wt.% C15A with PA 6, or PP + PP-MA as the matrix, plotted as functions of the degree of exfoliation

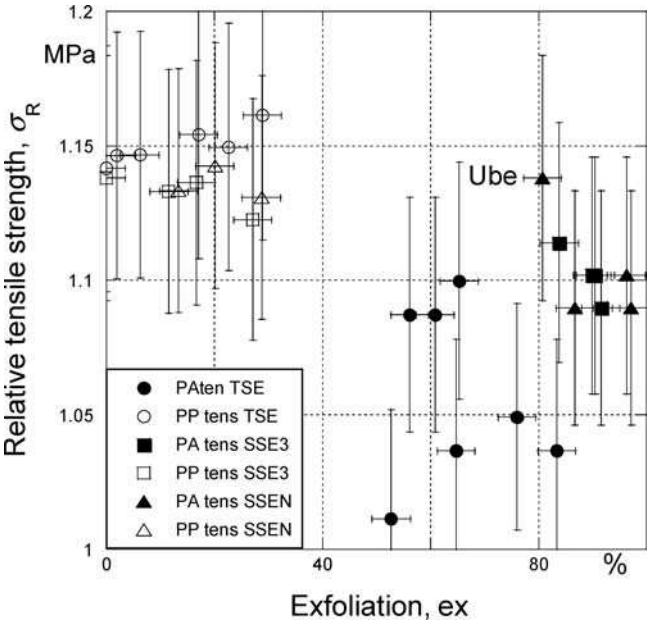

Fig. 13. Map of CPNC relative tensile strength vs. the degree of exfoliation. The samples were prepared in TSE, and SSE compounding lines with or without EFM

requires knowledge of clay tensile strength – in the present calculations that of mica [59], $\sigma_f = 240$ MPa, was used. The matrix tensile strength, σ_m, was measured using specimens extruded and molded the same way as the CPNC's. Substituting into Eq. 7 the true clay volume fractions in PP and PA 6 systems, $\varphi_f = 0.0042$ and 0.0053, respectively, resulted in under-prediction of σ_R. Since $\sigma_r \equiv \sigma_f/\sigma_m$ is well defined, the only possible cause is that a larger volume fraction of the reinforcing particles could originate from the solidification of polymer on clay surface [14 to 17].

The value of φ_f calculated for PP-type CPNC (assuming $\sigma_R = 1.15$) is 0.021 and that for PA 6 based CPNC (assuming $\sigma_R = 1.10$) is 0.049. Thus, this highly simplified analysis suggests that the volume of the reinforcing particles is about 5 and 9 times larger (for the PP-based and PA 6 type CPNC, respectively) than that calculated for the mineral alone. These numbers are not unreasonable [2], as the thickness of the adsorbed polymer layer has been reported to vary from about 3 to 6 nm – the former value for adsorption of PEG on deuterated PS [60], the latter for adsorption of PBD on mica [16]. However, to accept this hypothesis the results must be consistent with the information obtained from the tensile modulus. Halpin-Tsai (H-S) rigorously derived the relative tensile modulus in the stress direction:

$$E_R \equiv E_c/E_m = (1 + 2p\kappa\varphi_f)/(1 - \kappa\varphi_f)$$
$$\kappa = (E_r - 1)/(E_r + 2p); \quad E_r \equiv E_f/E_m, \tag{8}$$

with the same meaning of subscripts as in Eq 7. Here p is the aspect ratio defined as p = (platelet diameter)/(platelet thickness). For clay the values of modulus $E_f = 170$ GPa and the aspect ratio p = 295 may be used [2] – those of other parameters were already cited.

For the two CPNC with PA 6 or PP as the matrix Eq. 8 was used to calculate E_R from two models: #1 model assumed bare clay platelets dispersed in a polymer, and #2 model assumed that the platelets dispersed in the matrix are covered with solidified polymer. For model #1 the required parameters of Eq. 8 were used directly, e. g., for PA 6 system: $\varphi_f = 0.0053$, $E_f = 170$ GPa, and p = 295. However, since in model #2 the reinforcing particles comprise solidified layer of polymer, they need to be modified assuming volumetric additivity:

$$E_f' = (E_f + \xi E_m)/(\xi + 1)$$
$$p' = p/(\xi + 1) \quad , \tag{9}$$
$$\varphi_f' = \varphi_f(\xi + 1)$$

where the prime ($'$) indicates the modified parameters of Eq. 8, and ξ is the thickness of adsorbed polymer (in multiples of the clay platelet thickness). The results of calculations are not unexpected – both models gave similar prediction of the enhancement: for CPNC with PA 6 as the matrix, model #1 gave $E_R = 1.297$, while model #2 $E_R = 1.298$; for CPNC with PP as the matrix, model #1 gave $E_R = 1.371$, while model #2 $E_R = 1.372$. Algebraically, it is readily shown that the relative modulus of model #2 is:

$$\left.\begin{array}{l} E_R' = (1 + 2p\varphi_f\kappa')/(1 - \varphi_f'\kappa') \cong 1 + 2p\varphi_f\kappa' \\ \kappa' = [E_f + h(E_m - 1) - 1]/[E_f + hE_m + 2p] \\ E_f \gg E_m; \quad p \gg 1 \end{array}\right\} E_R' \cong E_R. \tag{10}$$

Conceptually, the equality of the two models is easy to understand. The solidification of polymer increases the volume of the reinforcing particles, but at the same time it reduces their aspect ratio and the ever-important modulus. In the recent monograph [2] several theoretical models have been discussed. However, only the Halpin-Tsai and equivalent models are readily applicable – the others either require empirical factors, or information about the filler-matrix interphase, and thus are not less suitable for predicting modulus enhancement.

Eqs. 8 to 10 gave $E_R \cong 1.3$ and 1.4 for CPNC with PA 6 and with PP as the matrix, respectively. The first prediction agrees with the experimental value $E_R \cong 1.31 \pm 0.05$ (see Fig. 12) for the exfoliated CPNC's with PA 6 as the matrix, extruded through SSE + EFM. However, for the PP-based CPNC's the Halpin-Tsai prediction is higher than the experimental value of $E_R \cong 1.20 \pm 0.05$, i. e., melt compounding of PP-based CPNC achieved only about $^1/_2$ of the theoretically possible enhancement. The reason for the disparity is obvious from the data shown in Fig. 11 – clay platelets in PP matrix have been poorly dispersed. Since it was shown above that the bare-clay model #1 provides the same prediction as the more realistic model #2, one may use Eq. 8 for extracting the empirical aspect ratio of $p \cong 44$. Accordingly, the thickness of a bulk-average reinforcing particle is $t \cong 6.7$ nm, and since $d_{001} \cong 3.3$ nm, the number of clay platelets in it is $N \cong 3$, in agreement with the XRD findings.

For the studied nanocomposites the tendency for E_R and σ is similar. In both cases the data form three clusters: one for PP-based CPNC, and two for PA-based CPNC prepared in a TSE and in SSE compounding line. In the latter case EFM-N engenders better exfoliation than EFM-3, but this has little effect on strength. Closer analysis reveals that there is a linear re-

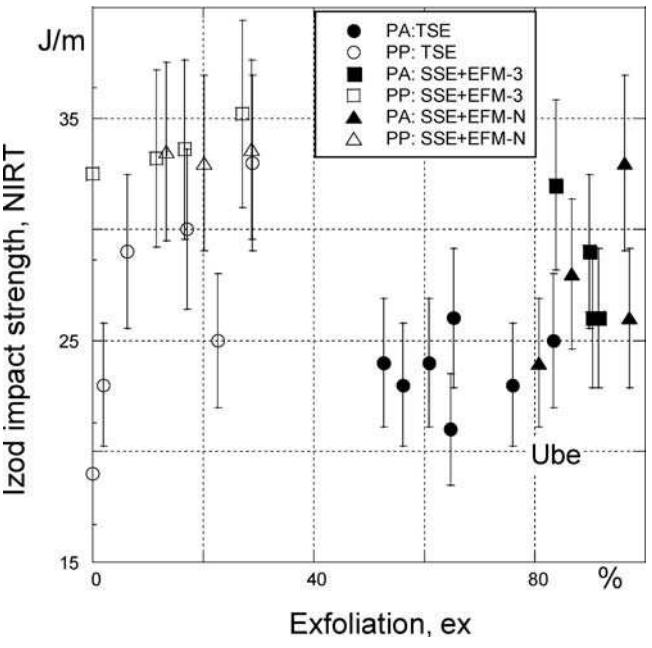

Fig. 14. Notched Izod impact strength at room temperature (NIRT) vs. the degree of exfoliation for CPNC samples with PP and PA 6 matrix. For comparison, the value for the commercial Ube PA1015C2 is also shown

lation between the tensile modulus and strength. The strength of PP-based CPNC is almost independent of ex, or the compounding method – similar from the TSE + EFM and SSE + EFM compounding lines.

Finally, Fig. 14 displays the impact strength at room temperature (NIRT), as a function of ex. As before, the data fall into three groups. Within the PP group the results from TSE show poor performance while these from SSE + EFM a slightly better one; there is no clear difference between EFM-3 and EFM-N. However, closing the C-D gap in either EFM improved exfoliation and NIRT. Similarly, for the PA 6 type CPNC's, compounding in TSE resulted in low exfoliation and poor impact strength, while that in SSE + EFM in better performance. For these nanocomposites the advantage of EFM-N is evident. Frequently NIRT and E showed the opposite tendencies, e. g., NIRT (kJ/m^2) = 6.63 – 2.39E (GPa) for a series of PA-based CPNC's [61]. A similar tendency is seen in the data for PA 6/C15A prepared in a specific compounding line, viz. good correlation is observed between NIRT and E extruded using either TSE or SSE, but not when the data from these two sets are combined.

In Figs. 12 to 14 the results obtained for Ube PA1015C2 nanocomposite are also plotted. As reported in Table 5, this material showed the highest value of the tensile and flexural modulus and strength, but the values for the compounded PA 6/C15A were within the experimental error. However, Ube PA1015C2 has relatively poor impact strength. The difference in mechanical behavior of the Ube material and PA 6/C15A is most likely related to the clay-matrix interphase (the matrix molecular weight is the same). In reactively prepared Ube PA1015C2 there is a direct ionic bonding of clay platelets to the matrix, whereas in PA 6/C15A there is only a partial interaction of unspecified nature (probably via hydrogen bonding). Furthermore, in the latter system the clay surface remains partially covered by the immiscible with PA 6 paraffin intercalant. As a result of these two factors the PA 6/C15A is less rigid, but tougher than the commercial CPNC from Ube.

6 Conclusions

Two types of CPNC, one based on PA 6 and the other on PP, were melt-intercalated in compounding lines consisting of either TSE with GP and EFM, or SSE with EFM. Mixing capabilities of two types of EFM were compared, one being a commercial mixer designed for polymer blends, the other designed for dispersing nano-particles. Several process variables were studied, viz., temperature, screw speed, throughput, method of extruder feeding, composition, organoclays, compatibilizers, pressure inside EFM, gap between the C-D plates, etc. The two compounding lines, with TSE or SSE, were compared at the same throughput of Q = 5 or 10 kg/h. This resulted in a significant difference in the residence time – while in the TSE the EFM gap setting caused variation of the peak residence time from t_R = 139 to 368 s, in the SSE the residence time was constant, but longer, t_R = 1140 or 570 s for Q = 5 or 10 kg/h, respectively. However, the degree of clay dispersion was found to mainly depend on the C-D gap in EFM. For brevity, in this article only one assembly for TSE and SSE, and limited number of C-D gap settings were presented. Similarly, only limited information on the clay dispersion and CPNC performance are given. This summary is illustrated with representative data.

The mechanism of organoclay (C15A) dispersion involves two steps: (1) a partial elimination of the intercalant from the clay surface, followed by (2) clay-matrix interaction. In the case of PA 6 the latter process involves direct adsorption of the polar macromolecules on the partially bare clay surface, whereas in the case of PP it is bonding of MAH groups of the PP-MA compatibilizers to the clay surface. The role of compounding is to facilitate the access of the polar macromolecular species to the bare clay surface. EFM was found to be efficient in peeling individual lamellae from the short stacks. Evidently, for full exfoliation the diffusion rate of reactive macromolecule to the clay surface must be higher than that of clay platelets reaggregation. The compounding lines differently affect these processes – TSE seems to cause more intercalant degradation than SSE.

Melt compounding PA 6/C15A in the SSE + EFM engendered the highest level of clay dispersion – comparable or better than that in commercial Ube-PA1015C2. In TSE + GP + EFM the degree of dispersion was significantly poorer than in SSE + EFM. Results for the PP-based CPNC's were less impressive. However, again better dispersion was obtained in SSE + EFM than TSE + GP + EFM. In the former line, as the EFM gap was reduced down to 30 μm, d_{001} remained relatively constant, while the degree of exfoliation. However, in the TSE compounding line, d_{001} systematically decreased with reduction of the EFM gap, while the aggregates (with interlamellar spacing $d_{001} \cong 1.35 \pm 0.01$ nm) increased. Both CPNC systems compounded with EFM-N had a higher degree of dispersion than these using the commercial EFM-3. At the same small gap between the C-D plates (h = 15 and 30 μm for PP and for PA 6 based nanocomposites, respectively) the level of exfoliation was the highest.

If the organoclay is well dispersed, then one must expect good mechanical performance, viz. at 2 wt.% organoclay loading the Young's modulus should be about 23 %, and the tensile strength by 10 to 15 % higher than that of the matrix. This enhancement was indeed obtained for the exfoliated PA 6 type CPNC. The intercalated PP-based nanocomposites showed lower than theoretically predicted mechanical performance. Analysis of the tensile strength at yield data indicated higher level of strength enhancement than theoretically predicted. The disparity indicates solidification of the matrix polymer on the clay surface, which greatly increases the volume of the dispersed solid particles.

References

1 *Okada, A., Usuki, A.:* Mater. Sci. Eng. C 3 (2), 109 (1995)
2 *Utracki, L. A.:* Clay-Containing Polymeric Nanocomposites. RAPRA, Shawbury, Shrewsbury, Shropshire UK (2004)
3 *Utracki, L. A.* (Ed.): Polymer Blends Handbook. Kluwer, Dordrecht (2002)
4 *Brauer, S.:* Polymer Nanocomposites: Nanoparticles, Nanoclays and Nanotubes. Business Communications Company Report P-234R (2004); *Ruban, L., S. Lomakin, Zaikov, G. E.:* Intern. J. Polym. Mater. 47, p. 117 (2000)
5 *Luciani, A., Utracki, L. A.:* Intern. Polym. Process. 11, p. 299 (1996); *Utracki, L. A., Luciani, A.:* Appl. Rheology 10(1), p. 10 (2000)

6 US Patent 5 451 106 (1995) *Nguyen, X. Q., Utracki, L. A.*; Canadian Patent Application 2 217 374 (1997) *Utracki, L. A., Luciani, A.*; PCT Patent Application WO 99/16540 (1999) *Utracki, L. A., Bourry, D., Luciani, A.*
7 Extensional Flow Mixer, Inc., Technical Information, 1999; http://www.futuresoft.net/efm
8 in 1999 IMI licensed the mixer to the Extensional Flow Mixer, Inc., for the manufacturing and distributing the EFM; the license was withdrawn in 2004
9 *White, J. L.:* Twin Screw Extruder Technology and Principles. Hanser, Munich (1990)
10 *Song, W.,* in: Mixing & Application of Polymer Nanocomposites. ITRI Publication No. D412KC2P00-8, Hsinchu, Taiwan (2002)
11 *Utracki, L. A.:* Paper Presented at International Conference PNC-2003, Boucherville, QC, Canada (2003)
12 *Tanoue, S., Utracki, L. A., Garcia-Rejon, A., Tatibouët, J., Cole, K. C., Kamal, M. R., Nassar, N.:* Paper presented at SPE-Asia, Nagoya, Japan (20039
13 *Manas-Zloczower, I., Tadmor, Z.* (Eds.): Mixing and Compounding of Polymers. Hanser, Munich (1994)
14 *Utracki, L. A., Simha, R., Garcia-Rejon, A.:* Macromolecules 36, p. 2114 (2003)
15 *Israelachvili, J. N.:* Intermolecular and Surface Forces with Applications to Colloidal and Biological Systems. Academic Press, New York (1985)
16 *Luengo, G., Schmitt, F.-J., Hill, R., Israelachvili, J. N.:* Macromolecules 30, p. 2482 (1997)
17 *Hentschke, R.:* Macromol. Theory Simul. 6, p. 287 (1997)
18 *Tanak, G., Goettler, L. A.:* Polymer 43, p. 541 (2002)
19 *Brown, D., Mélé, P., Marceau, S., Albérola, N. D.:* Macromolecules 36, p. 1395 (2003).
20 *Kim, K., Utracki, L. A., Kamal, M. R.:* J. Chem. Phys. 121, p. 10766 (2004)
21 *Manas-Zloczower, I.,* in: Mixing and Compounding of Polymers. *Manas-Zloczower, I., Tadmor, Z.* (Eds.), Hanser, Munich (1994)
22 *Dennis, H. R., Hunter, D. L., Chang, D., Kim, S., White, J. L., Cho, J. W., Paul, D. R.:* Polymer 42, p. 9513 (2001)
23 *Tucker III, C. L.,* in: Mixing in Polymer Processing. *Rauwendaal, C.* (Ed.), Marcel Dekker, New York (1991)
24 *Utracki, L. A., Shi Gerard, Z. H.,* in: Polymer Blends Handbook. Kluwer, Dordrecht (2002)
25 *Rauwendaal, C.:* Polymer Mixing. Hanser, Munich (1998)
26 *Song, W.:* SPE ANTEC Tech. Papers 46, p. 270 (2000)
27 *Nassar, N., Utracki, L. A., Kamal, M. R.:* Int. Polym. Process., submitted (2005)
28 US Patent 5 433 112 (1995) *Piché, L., Hamel, A., Gendron, R., Dumoulin, M. M., Tatibouët, J.*
29 *Tanoue, S., Utracki, L. A., Garcia-Rejon, A., Tatibouët, J., Cole, K. C., Kamal, M. R.:* Polym. Eng. Sci. 44, p. 1046 (2004)
30 US Patent 5 514 734 (1996) *Maxfield, MacRae, Christiani, B. R., Sastri, V. R.*
31 *Plueddemann, E. P.:* Silane Coupling Agents. Plenum Press, New York (1982)
32 Petrarch Systems, Silicon Compounds-Register and Review (1987)
33 *Liu, L., Qi, Z., Zhu, X.:* J. Appl. Polym. Sci. 71, p. 1133 (1999)
34 *Varlot, K., Reynaud, E., Kloppfer, M. H., Vigier, G., Varlet, J.:* J. Polym. Sci. Part B: Polym. Phys. 39, p. 1360 (2001)
35 *Davis, R. D., Bur, A. J., McBrearty, M., Lee, Y.-H., Gilman, J. W., Start, P. R.:* Polymer 45, p. 6487 (2004)
36 *Nair, S. S., Ramesh, C.:* Macromolecules 38, p. 454 (2005)
37 *Wu, S., Jiang, D., Ouyang, X., Wu, F., Shen, J.:* Polym. Eng. Sci. 44, p. 2070 (2004)
38 *Yu, Z.-Z., Yang, M., Zhang, Q., Zhao, C., Mai, Y.-W.:* J. Polym. Sci.: Part B: Polym. Phys. 41, p. 1234 (2003)
39 *Yu, Z.-Z., Yan, C., Yang, M., Mai, Y.-W.:* Polym. Int. 53, p. 1093 (2004)
40 *Chavarria, F., Paul, D. R.:* Polymer 45, p. 8501 (2004)
41 *Shah, R. K., Paul, D. R.:* Polymer 45, 2991 (2004)
42 Japan Kokai 109 998 (1976) *Fujiwara, S., Sakamoto, T.*
43 US Patent 4 739 007 (1988) *Okada, A., Fukushima, Y., Kawasumi, M., Inagaki, S., Usuki, A., Sugiyama, S., Kurauchi, T., Kamigaito, O.*
44 US Patent 5 973 053 (1999) *Usuki, A., Kato, M., Okada, A.*
45 *Kawasumi, M., Hasegawa, N., Kato, M., Usuki, A., Okada, A.:* Macromolecules 30, p. 6333 (1997)
46 *Usuki, A., Kato, M., Okada, A., Kurauchi, T.:* J. Appl. Polym. Sci. 63, p. 137 (1997)
47 *Kato, M., Usuki, A., Okada, A.:* J. Appl. Polym. Sci. 66, p. 1781 (1997)
48 *Hasegawa, N., Kawasumi, M., Kato, M., Usuki, A., Okada, A.:* J. Appl. Polym. Sci. 67, p. 87 (1998)
49 *Cole, K.:* personal communication (2004)
50 *Bureau, M. N., Perrin-Sarazin, F., Ton-That, M.-T.:* Polym. Eng. Sci. 44, p. 1142 (2004)
51 *Hasegawa, N., Okamoto, H., Kawasumi, M., Kato, M., Tsukigase, A., Usuki, A.:* Macromol. Mater. Eng. 280/281, p. 76 (2000); *Hasegawa, N., Okamoto, H., Kato, M., Usuki, A.:* J. Appl. Polym. Sci. 78, p. 1918 (2000)
52 *Hasegawa, N., Usuki, A.:* J. Appl. Polym. Sci. 93, p. 464 (2004)
53 *Hofmann, A. W.:* Liebigs Ann. Chem. 78, p. 253 (1851)
54 *Lee, J. W., Lim, Y. T., Park, O. O.:* Polym. Bull. 45, p. 191 (2000)
55 US Patent 5 102 948 (1992); EP 398 551 B1 (1995) *Deguchi, R., Nishio, T., Okada, A.*
56 Ube Industries, Ltd., Nylon Resin Dept.: High Performance Nylon Resin – Technical Data (Molding applications), March (2000)
57 *Bureau, M., Denault, J., Glowacz, F.:* SPE ANTEC Tech. Papers 47, p. 2125 (2001)
58 *McCrum, N. G., Buckley, C. P., Bucknall, C. B.:* Principles of Polymer Engineering, Oxford Sci. Pub., Oxford (1988)
59 *Milewski, J. V., Katz, H. S.* (Eds.): Handbook of Reinforcements for Plastics, Van Nostrand Reinhold, New York (1987)
60 *Cosgrove, T., Heath, T. G., Ryan, K., Crowley, T. L.:* Macromolecules 20, p. 2879 (1987)
61 US Patent 6 060 549 (2000) *Li, D.-M., Peiffer, D. G., Elspass, C. W., Wang, H.-C.*

Acknowledgments

The work described in this paper was in part carried out in collaboration with M. Tokihisa, K. Yakemoto, and T. Sakai, from the Japan Steel Works, Ltd., Hiroshima, Japan. The authors gratefully acknowledge their interest and support, as well as the help from staff of the NRCC/IMI, especially that from Dr. Jacques Tatibouët, Yves Simard, Florence Perrin, and Manon Plourde.

Date received: August 12, 2005
Date accepted: October 6, 2005